OH group behavior and pressure-induced amorphization of antigorite examined under high pressure and temperature using synchrotron infrared spectroscopy

NAOKI NOGUCHI,[1,*] TARO MORIWAKI,[2] YUKA IKEMOTO,[2] AND KEIJI SHINODA[1]

[1]Department of Geosciences, Graduate School of Science, Osaka City University, Sugimoto 3-3-138, Sumiyoshi-ku, Osaka 558-8585, Japan
[2]Japan Synchrotron Radiation Research Institute, 1-1-1 Mikazuki-cho, Sayo-gun, Hyogo 679-5198, Japan

ABSTRACT

Infrared (IR) absorption spectra of antigorite were measured up to 27 GPa and 320 °C using synchrotron IR radiation to elucidate OH group behavior under high-pressure (HP) and high-temperature (HT) conditions. The absorption bands attributable to the OH stretching modes of outer OH groups (OH_{outer}) and inner OH groups (OH_{inner}) show positive pressure dependencies. The shift rate of the OH_{inner} band is almost constant at all pressure ranges. In contrast, that of the OH_{outer} band increases slightly at about 6 GPa. This discontinuous change of the shift rate is consistent with the anomalous behavior of the OH_{outer} upon compression, which was predicted in the previous first-principle calculation study. Specifically, the pressure dependence of the OH_{outer} band shows that the hydrogen ion of an OH_{outer} interacts not only with the nearest basal oxygen ion of the SiO_4 tetrahedron but also with the second nearest two basal oxygen ions upon compression. The latter interaction becomes dominant over the former interaction at about 6 GPa.

Pressure-induced amorphization was indicated from IR spectra measured at 300 °C and 25.6 GPa. This *P-T* condition is out of the thermodynamic stability field of antigorite. A broad absorption band, which is close to the broad band attributable to natural hydrous silicate glass, appeared after amorphization, which suggests that the pressure-induced amorphization of antigorite does not induce dehydration. Hydrogen atoms are retained in amorphized antigorite as OH groups.

Keywords: Antigorite, high pressure, pressure-induced amorphization, synchrotron infrared spectroscopy, high-temperature diamond-anvil cell (HT-DAC)

INTRODUCTION

Serpentine minerals generally occur during the hydrothermal alteration of mantle peridotite, which forms the mantle wedge (Hyndman and Peacock 2003) or the subducting plate including the crust and upper mantle at the subduction zone (Ranero and Sallares 2004). Serpentine minerals in hydrated mantle peridotite are probable candidates as water carriers to the depth of subduction zones (e.g., Ulmer and Trommsdorff 1995; Iwamori 1998; Schmidt and Poli 1998). The free water supplied through the breakdown of the serpentine minerals in the depth of the subduction zone induces partial melting of the mantle wedge (Ulmer and Trommsdorff 1995). The breakdown of the serpentine minerals controls tectonic and seismic processes in the subduction zones (e.g., Hilairet et al. 2007; Chernak and Hirth 2010; Hirauchi et al. 2010). As such, knowledge of the stabilities and the physicochemical properties of the serpentine minerals under high-pressure (HP) and high-temperature (HT) conditions are necessary to construct a comprehensive model for water circulation in subduction zones. Previous experimental studies of serpentine minerals have revealed that antigorite has the largest stability field among serpentine minerals under HT conditions (Evans et al. 1976; Wunder and Schreyer 1997). Consequently,

antigorite must be abundant in the mantle wedge (Hyndman and Peacock 2003; Reynard et al. 2007; Katayama et al. 2009; Bezacier et al. 2010; Mookherjee and Capitani 2011). However, despite its importance for the fundamental properties of antigorite, details of the crystal structure—including the geometry of OH groups under HP–HT condition—remain unclear.

Figure 1a shows the basic structure of serpentine minerals consisting of a tri-octahedral sheet combined with a tetrahedral sheet, designated as the 1:1 layer, and OH groups of two types: OH_{outer} and OH_{inner}. The hydrogen ion of the OH_{outer} bonds to every surface oxygen ion of tri-octahedral sheets, and that of OH_{inner} bonds to oxygen ions of the opposite sides of the OH_{outer}. The geometry of the OH_{outer} was determined from neutron diffraction data for lizardite-1*T* at 8 K (Gregorkiewitz et al. 1996). It showed that the axis of the OH group tilts from the **c** axis slightly to the nearest neighboring oxygen ion of the tetrahedral sheet of the next 1:1 layer. The angle between the axis of the OH_{outer} and the line joining the hydrogen ion of the OH_{outer} to the nearest neighboring oxygen ion ($OH_{outer}\cdots O$ bond angle) at 8 K is 165.6° (Gregorkiewitz et al. 1996), which suggests that the OH_{outer}s form a weak hydrogen bond with oxygen ions. In contrast, the strength of the hydrogen bond of the OH_{inner} is weaker than that of the OH_{outer}, and the difference in the strength of the hydrogen bond can be inferred from the bond lengths of the OH groups: the bond length of OH_{inner} (0.80 Å) is shorter than that of the OH_{outer} (1.16 Å; Gregorkiewitz et al. 1996). In addition to the basic structure described above, modulation of the 1:1 layer is necessary for
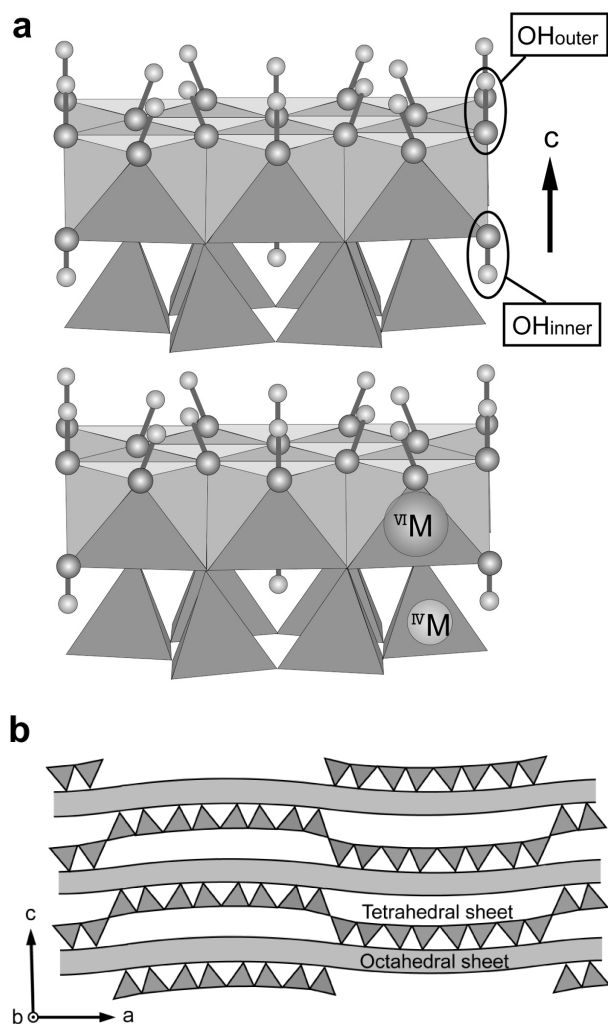
FIGURE 1. (**a**) Basic crystal structure of serpentine minerals. The schematic diagram is based on the positions of lizardite-1*T* (Mellini and Zanazzi 1989). The ^{VI}M and ^{IV}M sites are occupied, respectively, by Mg,Fe^{2+}, Ni,Mn^{2+}, and Si,Al. (**b**) Modulated crystal structure of antigorite along [010]. The OH groups are omitted from the diagram.

the crystal structures of serpentine minerals. The three principal polymorphs are derived from the modulation. Modulation of the 1:1 layer means that the layer polarity caused by the tetrahedral sheets changes in a certain wavelength along the **a** axis (Fig. 1b). The wavelength of modulation of natural typical antigorite ranges from 14 to 23 tetrahedra (Mellini et al. 1987). An experimental study (Wunder et al. 2001) revealed that the wavelength depends on the pressure–temperature (*P-T*) condition of its formation. In the antigorite crystal structure, the behavior of the OH groups and the modulation of the 1:1 layer under the HP–HT condition must play an important role for stabilizing the crystal structure.

In the current study, we measured IR absorption spectra of antigorite under HP–HT conditions with an external heating diamond-anvil cell (DAC) and synchrotron IR radiation. The behavior of the OH groups under HP–HT condition was deduced from the IR absorption spectra of the vibration of the OH groups.

In addition, pressure-induced amorphization was observed in the experiment at *P-T* conditions out of its thermodynamic stability field. The state of the OH groups in the amorphized antigorite is also reported in this paper.

EXPERIMENTAL METHODS

Sample characterization

A well-crystallized antigorite from Nakanochaya, Miyazu City, Kyoto Prefecture, Japan, whose crystallographic characteristics were described in Uehara and Shirozu (1985), was used as an experimental sample. It occurs as a polycrystalline aggregate comprising greenish, fibrous, 7 cm long bundles. The sample was confirmed as antigorite using powder X-ray diffraction measurements. According to Uehara and Shirozu (1985), the regular wavelength of undulation along the **a** axis was determined as 36.03 Å (M = 6.62, *b* = 9.21 Å, *c* = 7.28 Å, β = 91.33°) from the diffraction pattern. The chemical composition of the antigorite was determined using SEM-EDS (S-3500; Hitachi Ltd.). The average values were MgO = 39.58, SiO$_2$ = 42.84, Al$_2$O$_3$ = 1.64, FeO = 1.93 wt% (Total: 85.99 wt%).

High-pressure experiments

An externally heated DAC of a piston-cylinder type was used to generate pressure and temperature (Fig. 2). The DAC is equipped with a pair of type-Ia diamond anvils with a 600 μm diameter culet. Heaters of two types—a band heater and a coil heater—were used for heating the sample uniformly for many hours. A band heater surrounded the cylinder part, and a coil heater of a Kanthal wire 400 μm diameter surrounded the diamond anvil. It was fixed to the cylinder by a ceramic bond. The junction of a thermocouple was fixed on the surface of the diamond by the ceramic bond. To prevent thermal expansion of the coil heater during experiments, a ring of ceramic (Si$_3$N$_4$) enclosed the coil heater. The coil heater power was controlled using PID feedback based on the temperature measured using the thermocouple. A pre-indented Re foil with a sample hole of 200 μm diameter was used as gasket. The antigorite and KBr as pressure media were powdered and mixed well by grinding. Absorbed water was removed by heating the mixture for 12 h at 140 °C. The mixture of the powdered antigorite and KBr was loaded into the sample hole with SrB$_4$O$_7$: Sm^{2+} and ruby chips for pressure calibration. Powdered KBr, free of antigorite, was partially loaded in the sample hole as a reference space to transmit the reference light during measurement of the IR absorption spectra. The pressure
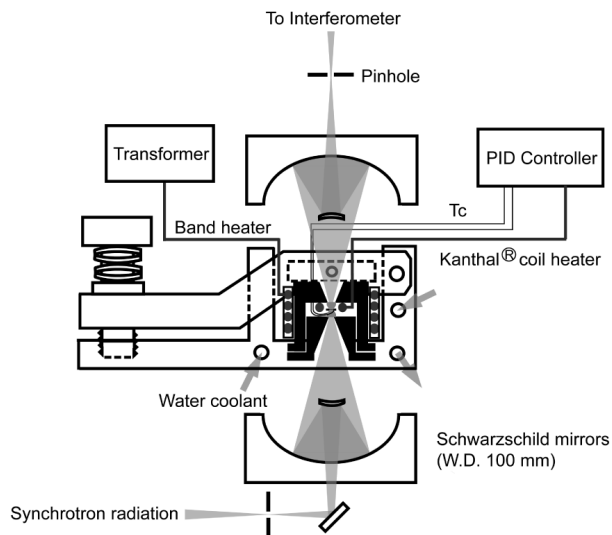

FIGURE 2. Schematic diagram of the external heating DAC under the synchrotron IR microscope. The DAC is composed with a stainless steel piston and a cylinder. A load is applied to the DAC using a lever-arm mechanism. The piston and cylinder parts are cut conically at an angle of 60° so that synchrotron IR light collected with the Schwarzschild mirrors is optimized for microscopic measurement. Water coolant is circulated through the lever-type pressure generator by a chiller.

and temperature in the sample hole were determined using two-sensor fluorescence technique with SrB_4O_7: Sm^{2+} and ruby (Datchi et al. 1997). The IR measurements were conducted under the IR microscope of BL43IR at Super Photon ring-8 GeV (SPring-8, Hyogo, Japan; Kimura et al. 2001; Shinoda et al. 2002). Absorption spectra of 800–6000 cm^{-1} were measured using 2 cm^{-1} resolution with a Fourier transform IR interferometer (IFS120HRX; Bruker Co.) equipped with a KBr beam splitter and a liquid-nitrogen-cooled HgCdTe detector. A 20 μm diameter pinhole was used as an aperture. Reference spectra were measured at the reference space in the sample hole whenever *P-T* condition was changed. Three experimental series with different *P-T* paths (Runs 1–3) were conducted with temperatures up to 320 °C and pressures up to 27 GPa (Fig. 3).

RESULTS

Peak-fitting analysis

Figures 4a and 4b, respectively portray selected spectra in the OH stretching frequency region of the Runs 1 and 2 under isothermal compression at 20 and 220 °C. In the ambient spectra (Fig. 4a), a weak broad band at 3562 cm^{-1} and an asymmetric intense band at 3680 cm^{-1} are observed, which suggests that several kinds of OH bands overlap in this region. The intense band seems to split into two bands at pressures greater than 14 GPa. The split seems to indicate an abrupt change of OH groups in antigorite under high pressure. However, the apparent split of the peak is revealed to result from the different pressure dependence of the several peaks, as determined by subsequent peak fitting. Therefore the split does not represent a phase transition such as decomposition or amorphization. To analyze the precise peak positions of the absorption bands, curve fitting of analyses of every absorption bands were performed using Lorentzian function with linear background correction using GRAMS/AI software (Thermo Galactic Inc.). The fitting parameters were the peak position and the full-width at half maximum (FWHM). The two parameters were not constrained during iterative calculations. According to previous Raman studies of serpentine
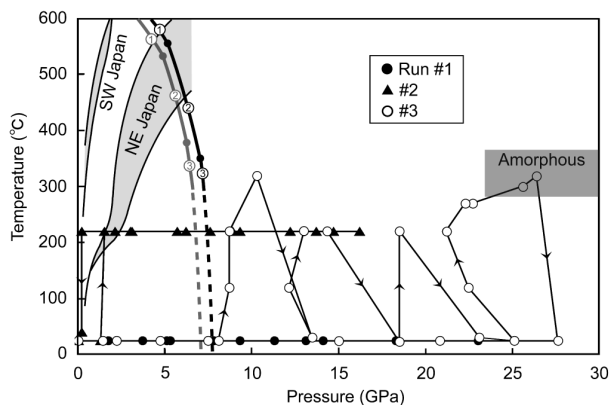
(Auzende et al. 2004; Reynard and Wunder 2006; Mizukami et al. 2007), we assumed in a first step four absorption bands between 3300 and 4000 cm^{-1}. Consequently, fitting analyses of each spectrum were apparently successful. However, the FWHMs of the separate peaks produced irregularly discontinuous trends against pressure even at intervals of 1 GPa. Because it is unreasonable that the FWHMs fluctuate irregularly in a
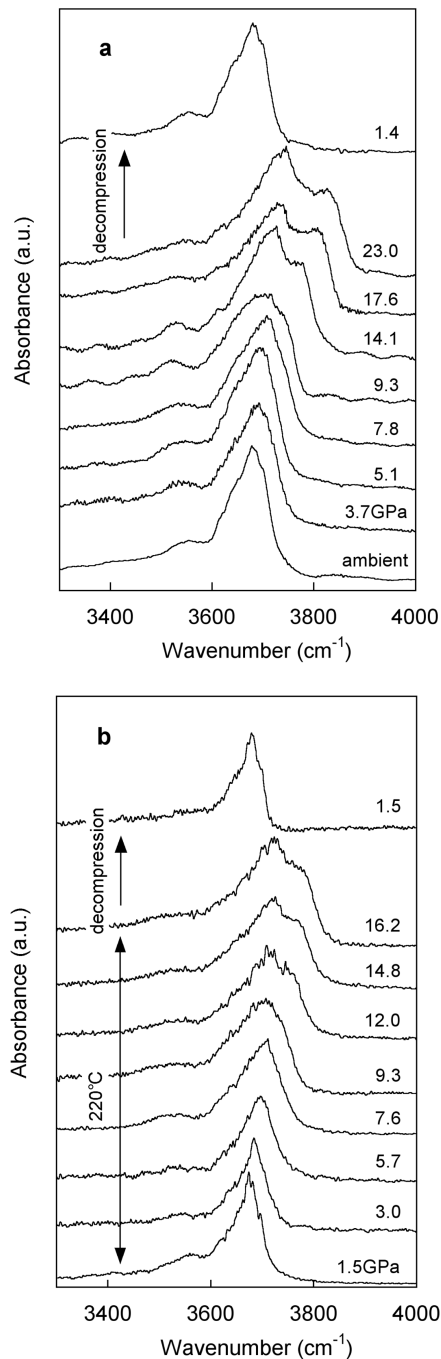

FIGURE 3. Experimental *P-T* paths from Runs 1 to 3. The dark-gray shaded area shows the *P-T* condition under which pressure-induced amorphization occurred in Run 3 (see the text). The reaction curves of antigorite determined by Nestola et al. (2009) and Hilairet et al. (2006) are shown as the black and gray lines, respectively. The reactions from 1 to 3 are: (1) antigorite = forsterite + talc + H_2O, (2) antigorite = enstatite + phase A + H_2O, (3) antigorite = talc + phase A + H_2O. The dashed lines are determined by extrapolation of the reaction curves of Nestola et al. (2009) and Hilairet et al. (2006). *P-T* conditions for oceanic crust subducting beneath northeast and southwest Japan calculated by Peacock and Wang (1999) are also shown as the light-gray shaded area.

FIGURE 4. Selected IR absorption spectra of antigorite obtained from isothermal compression experiments (Runs 1 and 2 in Fig. 3): (**a**) 20 °C and (**b**) 220 °C.

narrow pressure range and because the resulting peak positions must not be reliable, we abandoned the four-peak model. Next, assuming five peaks, we obtained successful fitting of every spectrum (e.g., Fig. 5) with a continuous peak shift of each fitted peak against pressure. Figure 6 shows the pressure dependence of five peak positions at 20 °C (filled) and 220 °C (open), which were reversible as a function of pressure. Peak positions of five bands are 3542 cm^{-1} (ν_1), 3630 cm^{-1} (ν_2), 3656 cm^{-1} (ν_3), 3680 cm^{-1} (ν_4), and 3702 cm^{-1} (ν_5) at ambient pressure. Although the 3542 cm^{-1} band (ν_1) shifts to lower wavenumbers up to about 9 GPa, four bands composing the intense asymmetric band shift to higher wavenumbers with increasing pressure (Fig. 6). The rates of wavenumber shift of five peaks are presented in Table 1. It is noteworthy that the shift rate of the 3680 cm^{-1} band (ν_4) at 20 and 220 °C increases discontinuously at 5.3 and 6.2 GPa, respectively, and that the shift rate of the ν_1 band changed from negative to positive at about 9 GPa.

The amorphization of antigorite can be interpreted in the spectra of Run 3, where the highest *P-T* condition in the three runs was attained (Fig. 3). Figure 7 portrays selected IR spectra obtained in Run 3. A broad absorption band appeared at wavenumbers 2800–3700 cm^{-1} at 300 °C and 25.6 GPa. The absorbance of the new broad band gradually grew as the *P-T* condition was maintained (Fig. 7). The sharp band at 3737 cm^{-1}, which is assigned to the normal mode of antigorite, overlapped with the broad band. It was gradually buried in the broad band over time. When the broad band appeared, absorption bands attributable to the combination mode of H_2O molecule did not appear around 5200 cm^{-1} (Fig. 7). Upon decompression, the absorbance of the broad band decreased rapidly when the *P-T* condition returned to the stable field (below about 8 GPa; Fig. 3); then the broad band disappeared at ambient condition (Fig. 7). The reasons why Figure 7 depicts the amorphization of antigorite are explained in a later section.

Autocorrelation analysis

We conducted autocorrelation analyses for all IR spectra to evaluate, quantitatively, the degree of amorphization of antigorite in the Run 3. The autocorrelation analysis enables parameterization of the effective line widths of absorption bands in IR spectra (Salje et al. 2000) with no peak fitting of raw spectra. It is particularly effective for analysis of absorption bands where a peak-fitting model cannot be constructed, such as the broad bands appearing in the spectra of Run 3 (Fig. 7). According to the procedure described in Salje et al. (2000), the autocorrelation analysis was performed as described below.

A segment from 2750 to 4000 cm^{-1}, which is OH stretching region, was extracted from each spectrum of antigorite. Then the background was subtracted from each segment. Consequently, both end points of the segment are on the linear baseline. The line widths of the bands in the segment are evaluated using the autocorrelation function defined as the following:

$$\mathrm{Corr}(a, \nu') = \int_{-\infty}^{\infty} a(\nu + \nu') a(\nu) d\nu$$

where $a(\nu)$ is the absorbance of the spectrum after baseline subtraction, which is expressed as a function of the wavenumber ν. The main information for the line width of the spectrum is
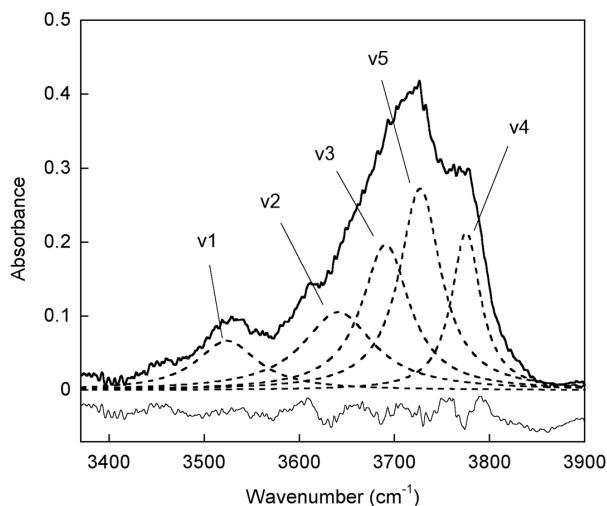

FIGURE 5. Peak fitting model of the IR spectrum of antigorite under HP–HT condition. The raw IR spectra in the OH stretching frequency region at 20 °C and 14.1 GPa (thin solid line) can be deconvoluted into five bands (dotted lines). The lowermost line shows residual errors.
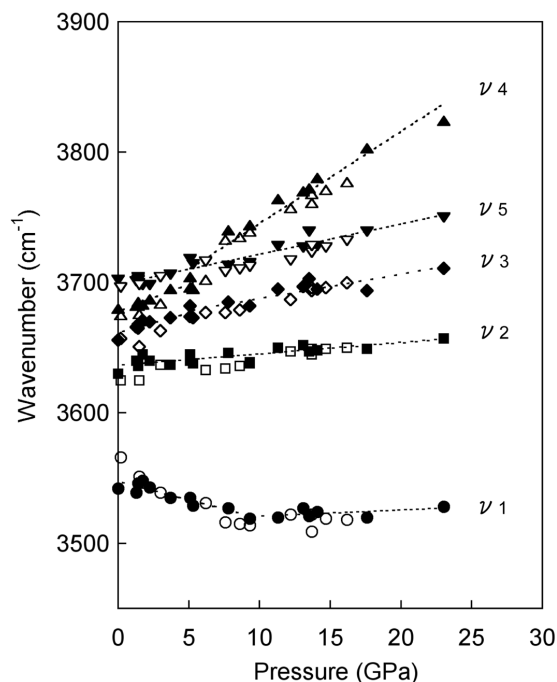

FIGURE 6. Pressure dependence of the peak positions of five absorption bands in the OH stretching frequency region. Isothermal compression data at 20 °C (Fig. 4a) and 220 °C (Fig. 4b) are shown, respectively, as closed and open symbols. Eye-guide lines are inserted into the data at 20 °C.

included in the shape of the central peak of the autocorrelation function, in the limit $\nu' \rightarrow 0$. The central peak shape can be treated quantitatively by fitting a Gaussian curve to the central peak around $\nu' = 0$. As a result of the Gaussian fitting analysis, the $\Delta Corr$ value is estimated. The $\Delta Corr$ value relates to the aver-

TABLE 1. Ambient frequencies and pressure derivatives of OH stretching bands of antigorite

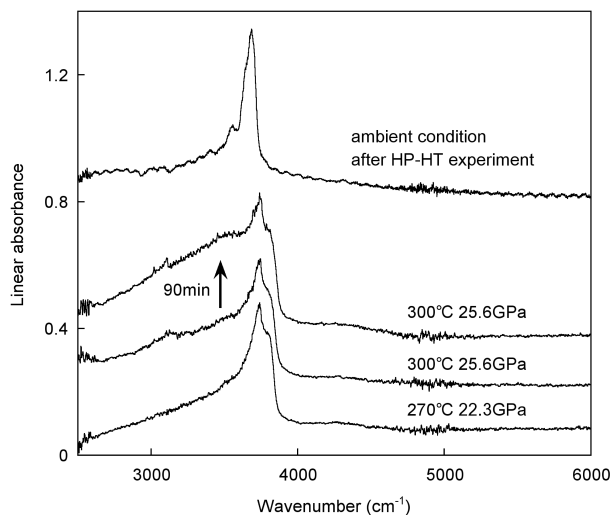| v_i (cm^{-1})	20 °C $(\partial v_i/\partial P)_T$ (cm^{-1}/GPa)		220 °C $(\partial v_i/\partial P)_T$ (cm^{-1}/GPa)		Mode assignment*
	(0 < *P* ≤ 9.0 GPa)	(9.0 < *P* ≤ 23.0 GPa)	(0 < *P* ≤ 9.0 GPa)	(9.0 < *P* ≤ 16.2 GPa)	
3542 (v_1)	−2.8	0.4	−5.6	0.4	OH$_{outer}$···O(SiAl)
	(0 < *P* ≤ 5.3 GPa)	(5.3 < *P* ≤ 23.0 GPa)	(0 < *P* ≤ 6.2 GPa)	(6.2 < *P* ≤ 16.2 GPa)	
3630 (v_2)	0.7	0.8	1.6	1.9	(MgMgFe)-OH
3656 (v_3)	2.6	1.6	3.4	2.8	(MgMgFe)-OH
3680 (v_4)	4.1	7.1	3.3	5.9	OH$_{outer}$···O(SiSi)
3702 (v_5)	2.4	2.4	1.2	2.8	OH$_{inner}$

* See text.

FIGURE 7. Selected IR spectra from Run 3. The spectrum at 270 °C and 22.3 GPa is obtained immediately before the *P-T* condition where the pressure-induced amorphization occurred (300 °C, 25.6 GPa). A broad absorption band attributable to pressure-induced amorphization appeared at wavenumbers of 2700–3600 cm^{-1} in the spectrum at 300 °C and 25.6 GPa. The absorbance of the broad band increased during 90 min.
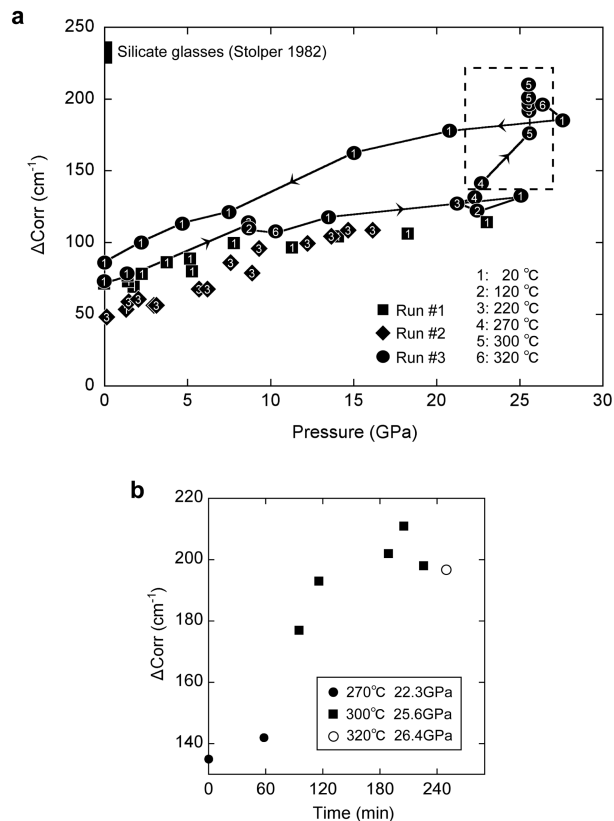

FIGURE 8. (a) Δ*Corr* of antigorite shown against pressure. They were determined by application of autocorrelation analysis (Salje et al. 2000) to segments of 2750–4000 cm^{-1} in each spectrum. The Δ*Corr* values of the OH stretching bands of natural and synthetic hydrous silicate (rhyolitic) glasses (Fig. 1 in Stolper 1982) are 225–240 cm^{-1} (bold bar). **(b)** Δ*Corr* included in the region enclosed by the dashed line in **a**.

age line width and splitting of absorption bands in the segment (Salje et al. 2000). The Δ*Corr* values for the spectra of antigorite are presented in Figure 8a. In addition to providing the standard of amorphization, the Δ*Corr* values of OH stretching bands of hydrous silicate glasses were containing from the IR spectra of natural rhyolitic glasses containing 0.12–1.89 wt% water (Stolper 1982); its range is presented in Figure 8a.

Comparison of Δ*Corr* of Run 3 with those of Runs 1 and 2 (Fig. 8a) shows that the behavior of the Δ*Corr* in Run 3 is markedly anomalous. In the compression process of Run 3, Δ*Corr* increases slightly with pressure up to about 25 GPa. This behavior is consistent with the trends of the Runs 1 and 2. However, Δ*Corr* of Run 3 increases drastically at 300 °C and 25.6 GPa. This drastic change corresponds to the appearance of the broad band and its growth in Figure 7. Figure 8b shows kinetic developments of Δ*Corr* at 300 °C and 25.6 GPa in Run 3. The Δ*Corr* increased suddenly when the *P-T* condition was changed from 270 °C and 22.3 GPa to 300 °C and 25.6 GPa. Then Δ*Corr* increased gradually and saturated after about 120 min after the last increase of the *P-T* condition. Furthermore, although the *P-T* condition was changed to 320 °C and 26.4 GPa, the Δ*Corr* value was constant. Upon decompression (Fig. 8a), Δ*Corr* gradually decreased and finally returned to a value that was slightly greater than that before the experiment.

DISCUSSION

Mode assignment for OH bands

Because the unit cell of the antigorite structure includes many atoms, the appearance of many absorption bands is allowed according to the rule for number of optical normal mode, as $3N - 3$, where *N* is the number of atoms in a unit cell. Because it is difficult to assign the observed absorption bands of antigorite to the intrinsic normal mode by the factor group analysis, we

assigned the five bands (ν_1–ν_5) by referring to the theoretical assignment of lizardite-1*T* (Balan et al. 2002). Based on the structural similarity between antigorite and lizardite, the mode assignments of antigorite is justified for the main absorption bands in the measured IR spectra based on previous studies for the IR spectrum of lizardite. The five IR absorption bands of antigorite are caused by stretching modes of the OH groups in the curved 1:1 layer, which is approximately the same as the lizardite structure. The stretching mode of the OH groups on the ends of the curved 1:1 layer, where the layer polarity switches, can be ignored because the curved 1:1 layer is long. Balan et al. (2002) determined the theoretical IR spectrum of lizardite-1*T* with first-principles calculation and assigned theoretical absorption bands to an IR spectrum of a natural lizardite-1*T*. They assigned two bands at 3684 and 3703 cm^{-1} in the natural lizardite-1*T* to in-phase stretching mode of OH_{outer}s and stretching mode of OH_{inner}s, respectively. Based on the band assignment of lizardite-1*T*, the 3680 cm^{-1} (ν_4) and 3702 cm^{-1} (ν_5) bands of antigorite at ambient can be assigned to the in-phase stretching modes of OH_{outer}s and the OH_{inner}s stretching mode, respectively (Table 1).

We estimate that the 3630 cm^{-1} (ν_2) and 3656 cm^{-1} (ν_3) bands are caused by the OH_{outer} and OH_{inner} bonded to the octahedra where Fe^{2+} substitutes Mg^{2+}. For clinoamphiboles, Burns and Strens (1966) showed that the stretching frequency of the OH group coordinated by two Mg^{2+} and one Fe^{2+} in the octahedral sites is about 15 cm^{-1} lower than that of the OH group coordinated by three Mg^{2+}. This effect of the substitution of Fe^{2+} on the OH stretching frequency results from the difference of the electronegativity between Mg^{2+} and Fe^{2+} (Burns and Strens 1966; Reynard and Wunder 2006). Consequently, the Fe^{2+} included in antigorite might lower of the stretching frequencies of the OH_{inner} or OH_{outer}.

The 3542 cm^{-1} band (ν_1) must be attributed to the minor amount of Al^{3+} substituting for Si^{4+} in tetrahedral sites, as suggested in previous studies (Serna et al. 1979; Uehara and Shirozu 1985). Results of these studies indicated that the band has a positive correlation between the absorbance of the 3562 cm^{-1} band and the Al^{3+} content. The substitution of Si^{4+} in a tetrahedron by Al^{3+} must yield excess electrons on the basal oxygen ions of the tetrahedron. That excess of electrons enhances hydrogen bonds between those of the basal oxygen ions and the hydrogen ion of the adjacent OH_{outer}. Consequently, the excess electrons lower the stretching frequency of the OH_{outer}.

Behaviors of OH groups at high pressure

Based on the mode assignment for the OH bands and their pressure dependence, we can discuss the behavior of the OH groups at high pressure in this section. The stretching frequency of OH group in hydrous minerals is sensitive to interaction with the atoms around the hydrogen ion. Particularly, it depends on the hydrogen bond geometry. Empirical relations between the stretching frequency and the OH···O bond distance or the OH···O bond angle indicate that a lengthened OH···O bond distance or a bent OH···O angle induces a greater shift (Nakamoto et al. 1955; Libowitzky 1999). Consequently, the stretching frequency of an OH group gives a crystallographic indication for the strength of the associated hydrogen bond. The fact that the OH_{outer} stretching bands (ν_4) and the OH_{inner} stretching band (ν_5) of antigorite have

positive pressure dependence (Table 1) apparently indicates that their hydrogen bonds were not enhanced under pressure. Past HP Raman studies of serpentine (Auzende et al. 2004; Reynard and Wunder 2006; Mizukami et al. 2007) also showed that the OH stretching Raman bands of the polymorphs of serpentine have positive pressure dependencies. However, the HP X-ray diffraction measurement using a single crystal of lizardite-1*T* (Mellini and Zanazzi 1989) reported the interlayer spacing to be shortened with pressure. Accordingly, the distance between the oxygen ion of an OH_{outer} and the nearest basal oxygen ion of a tetrahedron is shortened under pressure. In general, in hydrous minerals under pressure, the OH···O bond distance is shortened with shortening of the distance between the oxygen ion of the acceptor and that of the donor (O···O distance). The pressure dependence of the OH_{outer} stretching band (ν_4) of antigorite, however, does not indicate a shortening of the OH_{outer}···O bond distance. The only possible reason why the OH_{outer} shifts to the higher wavenumbers without lengthening of OH···O distance is the decrease of the OH_{outer}···O bond angle under pressure, specifically meaning that the OH_{outer} tilts toward or away from the center of the hexagonal ring formed by the SiO_4 tetrahedra ring. Assuming that the OH_{outer} tilts away from the center of the hexagonal ring, the OH_{outer}···O bond angle increases to 180°; then it begins to decrease. However, this is not consistent with the fact that the OH_{outer} stretching band (ν_4) never shifts to lower wavenumbers. Consequently, the OH_{outer}···O bond angle decreases with shortening the O···O distance so that the OH_{outer} tilts toward the center of the hexagonal ring (Fig. 9).

Why do the OH_{outer}s tilt to the center of the hexagonal rings? The first-principle calculation study for lizardite by Mookherjee and Stixrude (2009) proposed an answer for the problem. They predicted that lizardite-1*T* is so deformed under pressure that the misfit between octahedral and tetrahedral layers is cancelled. Specifically, when a SiO_4 tetrahedron rotates about the **c** axis, the adjacent tetrahedron rotates in opposite sense under pressure. Consequently, the hexagonal tetrahedral ring changes gradually to a ditrigonal ring. Because the tetrahedral ring is deformed, the distances between the hydrogen ion of an OH_{outer} and the second nearest two basal oxygen ions of the tetrahedron are shortened (Fig. 9). Mookherjee and Stixrude (2009) predicted that interactions between the hydrogen ion and the second nearest oxygen ions are strengthened, and that they come to compete with the hydrogen bond with the nearest oxygen ion at 0.4 GPa with the distance shortened. Consequently, for compression greater than 0.4 GPa, the OH_{outer} begins to tilt toward the center of the tetrahedral ring, and the OH_{outer}···O bond angle decreases (Mookherjee and Stixrude 2009). The positive shift rate of the OH_{outer} stretching band (ν_4) supports the result of the first-principle calculation. Furthermore, the fact that the shift rate of the ν_4 band increases slightly around 6 GPa must indicate that the interactions between the hydrogen ion and the second nearest two basal oxygen ion overcome that between the hydrogen ion and the nearest basal oxygen ion at pressure. The first-principle calculation has indeed predicted that the OH_{outer}···O bond angle increases abruptly at 7 GPa, which is confirmed experimentally by our result.

For a proper discussion, we must take the subtle difference of the crystal structures between lizardite and antigorite into considerations. However, the close similarity of their crystal
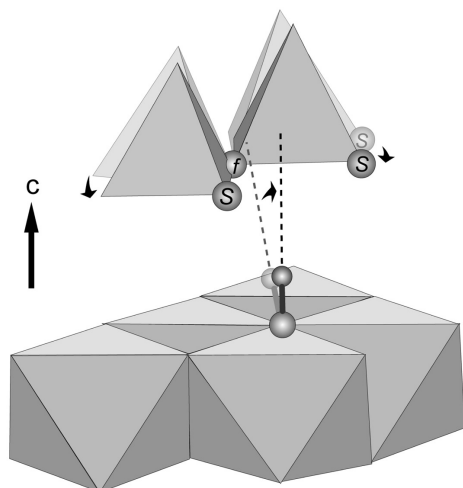
FIGURE 9. Change of the OH$_{outer}$ geometry with increasing pressure deduced from IR spectra at HP-HT conditions. The tetrahedral ring is also deformed, as portrayed in the figure, with tilting of the OH$_{outer}$. Interactions between the hydrogen ion of the OH$_{outer}$ and the second nearest oxygen ion, denoted as *s* in the figure, are enhanced by tetrahedral ring deformation. Interactions with the second nearest oxygen ions overcome the interaction with the first nearest oxygen ion, denoted as *f* in the figure, at about 6 GPa (see the text).

structure allows the interpretation of these experimental results of antigorite from the calculation of lizardite. In fact, the recent study for elastic property of antigorite under pressure by first-principle calculation (Mookherjee and Capitani 2011) proved that the compression behavior of antiogorite is very similar to that of lizardite. The study predicted that an anomalous change of the elastic constants occurs at about 6 GPa, similar to the predicted the anomalous change of lizardite at 7 GPa (Mookherjee and Stixrude 2009). Moreover, a HP X-ray diffraction study of antigorite (Nestola et al. 2009) revealed that an anomalous softening occurred at 6 GPa because of the increase of the axial compressibility along the **c** axis. Our result supports that the anomalous softening at 6 GPa was induced by losing the equilibrium between the interactions of the hydrogen ion to the nearest and second nearest oxygen ions.

However, the OH$_{inner}$ stretching band (ν_5) has an almost constant shift rate. The shift rate resembles that of the IR absorption band attributable to the OH stretching mode of talc: 2.1 cm^{-1}/GPa (Scott et al. 2007). That rate characteristic is expected because of the similarity between the structural environments around the OH group in talc and the one around the OH$_{inner}$ of serpentine. The structure around the OH$_{inner}$ must be compressed with the same mechanism as in talc. Consequently, the explanation for the positive shift rate of the OH$_{inner}$ stretching band is given by the pressure-induced increase in repulsion between the silicon cation and the hydrogen ion, as in the case of the OH group in talc (Mizukami et al. 2007; Scott et al. 2007).

The ν_1 band attributable to stretching modes of OH$_{outer}$s adjacent to tetrahedra occupied by Al^{3+} has negative pressure dependence (Table 1). Consequently, the hydrogen bond between the OH$_{outer}$ and that of the basal oxygen ions of the AlO$_4$ tetrahedron is enhanced under pressure. Velde and Martinez (1981)

also demonstrated that the OH$_{outer}$ stretching frequency of highly aluminous serpentine (amesite) has a negative shift rate (–17 cm^{-1}/GPa) by IR spectroscopic measurements up to 0.9 GPa. Our results and theirs imply that the electrical charge of the basal oxygen ion, which serves as the accepter of the OH$_{outer}$···O hydrogen bond, decides whether the hydrogen bond enhances with shortening O···O distance. Furthermore, this effect of the Al^{3+} substitution on the hydrogen bond gives a crystallographic interpretation for the HP stability of antigorite in the MgO-Al$_2$O$_3$-SiO$_2$-H$_2$O (MASH) system. The experimental study by Bromiley and Pawley (2003) showed a few Al^{3+} substituting in antigorite stabilizes the antigorite structure at high *P-T* condition and expands the stability field relative to that of antigorite in the MgO-SiO$_2$-H$_2$O (MSH) system. This effect of Al^{3+} substitution on the HP stability is presumably attributable to the enhancement of the hydrogen bond at high pressure by the substitution in addition to minimizing structural misfit among the component octahedral and tetrahedral sheets as suggested by them.

Pressure-induced amorphization

The previous HP X-ray diffraction study using a multi-anvil apparatus (Irifune et al. 1996) reported that the amorphization of serpentine minerals, antigorite and lizardite, occurred at temperatures of 200 to 400 °C and pressures of 20 to 27 GPa. The *P-T* range of the amorphization covers the *P-T* range within which the new broad band appeared in the IR spectra of Run 3, 300 °C and 25.6 GPa (Fig. 7). The *P-T* conditions of the amorphization observed in this study and the multi-anvil study (Irifune et al. 1996) are not consistent with the *P-T* conditions of the amorphization reported in the previous study using a DAC (Meade and Jeanloz 1991). In the DAC study by Meade and Jeanloz (1991), the amorphization of serpentine was detected using acoustic emission techniques at pressures of 6 to 25 GPa and at temperatures of up to 600 °C. We, however, did not observe the amorphization at pressures of 6 to 25 GPa at temperatures of up to 300 °C. The inconsistent *P-T* conditions of the amorphization must result from deviatoric stress generated in the sample hole of DAC. Because a powdered KBr was used as a pressure medium in this study, deviatoric stress was considerably relaxed by annealing. In contrast, in the previous study no pressure medium was used (Meade and Jeanloz 1991); accordingly, large deviatoric stress must be generated. Such a deviatoric stress probably serves as the trigger of the pressure-induced amorphization under lower pressure, in addition to thermodynamical instability (Richet and Gillet 1997). The pressure-induced amorphization controlled by the deviatoric stress is also supported by an experimental study for portlandite, which has a layered structure similar to that of antigorite (Catalli et al. 2008).

The broad-band shape in Figure 7 resembles that of absorption bands attributable to OH groups included in natural hydrous silicate glasses (Stolper 1982). The $\Delta Corr$ value of the broad band at 300 °C and 25.6 GPa indeed approached that of hydrous silicate glasses over time (Figs. 8a and 8b). Comparison of $\Delta Corr$ values of the hydrous silicate glasses with that of antigorite supports the existence of disordered OH groups in the amorphized antigorite structure. The large band width must indicate various atomic distributions around OH groups within the amorphized structure and the loss of a long-range ordering of the antigorite structure.

A sharp band at 3737 cm^{-1} in the spectra at 300 °C and 25.6 GPa remains with the broad band because of the amorphization (Fig. 7). Judging from pressure dependencies of the peak positions of normal modes (Fig. 6), the band at 3737 cm^{-1} may result from the OH band, which was the OH$_{inner}$ stretching mode (ν_5) before amorphization. The 3737 cm^{-1} band sharpness indicates a limited variation of atomic distribution and survival of a short-range ordering around the OH group. In general, the IR spectroscopy is sensitive to the IR active short-range structure. This allowed to confirm that some OH groups survive between octahedral and tetrahedral sheets after amorphization of antigorite. Consequently, the amorphized antigorite does not lose hydrogen atoms in the structure but keeps them in the amorphized structure as disordered and relict OH groups.

A comparison of the *P-T* conditions for the amorphization of antigorite and the geotherm of a subducting oceanic crust is important in terms of the geophysics of subduction zones. The geotherms for the oceanic crust beneath northwest and southwest Japan calculated by Peacock and Wang (1999) are incorporated in Figure 3. The figure illustrates that the antigorite in the hydrated mantle peridotite surrounding subducting oceanic crusts is unlikely to undergo amorphization, since the geotherms are much warmer than the *P-T* condition of the amorphization. However, the relationship among *P* and *T* and deviatoric stress where the amorphization is induced is still not well understood. Further detailed examinations of the relationship among *P*, *T*, and deviatoric stress where the amorphization is induced, are required to determine whether or not the amorphization occurs in the actual subduction zones.

REFERENCES CITED

Auzende, A.L., Daniel, I., Reynard, B., Lemaire, C., and Guyot, F. (2004) High-pressure behavior of serpentine minerals: a Raman spectroscopic study. Physics and Chemistry of Minerals, 31, 269–277.

Balan, E., Saitta, A.M., Mauri, F., Lemaire, C., and Guyot, F. (2002) First-principles calculation of the infrared spectrum of lizardite. American Mineralogist, 87, 1286–1290.

Bezacier, L., Reynard, B., Bass, J.D., Sanchez-Valle, C., and Van de Moortèle, B. (2010) Elasticity of antigorite, seismic detection of serpentinites, and anisotropy in subduction zones. Earth and Planetary Science Letters, 289, 198–208.

Bromiley, G.D. and Pawley, A. (2003) The stability of antigorite in the systems MgO-SiO$_2$-H$_2$O (MSH) and MgO-Al$_2$O$_3$-SiO$_2$-H$_2$O (MASH): The effects of Al^{3+} substitution on high-pressure stability. American Mineralogist, 88, 99–108.

Burns, R.G. and Strens, R.G.J. (1966) Infrared study of the hydroxyl band in clinoamphiboles. Science, 153, 890–892.

Catalli, K., Shim, S.H., and Prakapenka, V.B. (2008) A crystalline-to-crystalline phase transition in Ca(OH)$_2$ at 8 GPa and room temperature. Geophysical Research Letters, 35, L05312, DOI: 10.1029/2007GL033062.

Chernak, L.J. and Hirth, G. (2010) Rheology of antigorite serpentinite at high temperature and pressure. Earth and Planetary Science Letters, 296, 23–33.

Datchi, F., LeToullec, R., and Loubeyre, P. (1997) Improved calibration of the SrB$_4$O$_7$:Sm^{2+} optical pressure gauge: Advantages at very high pressures and high temperatures. Journal of Applied Physics, 81, 3333–3345.

Evans, B.W., Johannes, W., Oterdoom, H., and Trommsdorff, V. (1976) Stability of chrysotile and antigorite in the serpentine multisystem. Schweizerische Mineralogidche, 56, 79–93.

Gregorkiewitz, M., Lebech, B., Mellini, M., and Viti, C. (1996) Hydrogen positions and thermal expansion in lizardite-1*T* from Elba: a low-temperature study using Rietveld refinement of neutron diffraction data. American

Mineralogist, 81, 1111–1116.

Hilairet, N., Daniel, I., and Reynard, B. (2006) Equation of state of antigorite, stability field of serpentines, and seismicity in subduction zone. Geophysical Research Letters, 33, L02302, DOI: 10.1029/2005GL02472.

Hilairet, N., Reynard, B., Wang, Y., Daniel, I., Merkel, S., Nishiyama, N., and Petitgirard, S. (2007) High-pressure creep of serpentine, interseismic deformation, and initiation of subduction. Science, 318, 1910–1913.

Hirauchi, K., Katayama, I., Uehara, S., Miyahara, M., and Takai, Y. (2010) Inhibition of subduction thrust earthquakes by low-temperature plastic flow in serpentine. Earth and Planetary Science Letters, 295, 349–357.

Hyndman, R.D. and Peacock, S.M. (2003) Serpentinization of the forearc mantle. Earth and Planetary Science Letters, 212, 417–432.

Irifune, T., Kuroda, K., Funamori, N., Uchida, T., Yagi, T., Inoue, T., and Miyajima, N. (1996) Amorphization of serpentine at high pressure and high temperature. Science, 272, 1468–1470.

Iwamori, H. (1998) Transportation of H$_2$O and melting in subduction zones. Earth and Planet Science Letters, 160, 65–80.

Katayama, I., Hirauchi, K., Michibayashi, K., and Ando, J. (2009) Trench-parallel anisotorpy produced by serpentine deformation in the hydrated mantle wedge. Nature, 461, 1114–1118.

Kimura, S., Nanba, T., Sada, T., Okuno, M., Matsunami, M., Shinoda, K., Kimura, H., Moriwaki, T., Yamakata, M., Kondo, Y., and others. (2001) Infrared spectromicroscopy and magneto-optical imaging stations at SPring-8. Nuclear Instruments and Methods, 467–468, 893–896.

Libowitzky, E. (1999) Correlation of O-H-stretching frequencies and O···H-O hydrogen bond lengths in minerals. Monatshefte für Chemie, 130, 1047–1059.

Meade, C. and Jeanloz, R. (1991) Deep-focus earthquakes and recycling of water into the Earth's mantle. Science, 252, 68–72.

Mellini, M., Trommsdorff, V., and Compagnoni, R. (1987) Antigorite polysomatism: Behaviour during progressive metamorphism. Contributions to Mineralogy and Petrology, 97, 147–155.

Mellini, M. and Zanazzi, P.F. (1989) Effects of pressure on the structure of lizardite 1*T*. European Journal of Mineralogy, 1, 13–19.

Mizukami, T., Kagi, H., Wallis, S.R., and Fukura, S. (2007) Pressure-induced change in compressional behavior of the O–H bond in chrysotile: a Raman high-pressure study up to 4.5 GPa. American Mineralogist, 92, 1456–1463.

Mookherjee, M. and Capitani, G.C. (2011) Trench parallel anisotropy and large delay times: Elasticity and anisotropy of anigorite at high pressures. Geophysical Research Letters, 38, L09315, DOI: 10.1029/2011GL047160.

Mookherjee, M. and Stixrude, L. (2009) Structure and elasticity of serpentine at high-pressure. Earth and Planetary Science Letters, 279, 11–19.

Nakamoto, K., Margoshes, M., and Rundle, R.E. (1955) Stretching frequencies as a function of distances in hydrogen bond. Journal of American Chemical Society, 77, 6480–6486.

Nestola, F., Angel, R.J., Zhao, J., Garrido, C.J., Sánchez-Vizcaíno, V.L., Capitani, G.C., and Mellini, M. (2009) Antigorite equation of state and anomalous softening at 6 GPa: an in situ single-crystal X-ray diffraction study. Contributions to Mineralogy and Petrology, 160, 33–43.

Peacock, S.M. and Wang, K. (1999) Seismic consequences of warm versus cool subduction metamorphism: Examples from southwest and northeast Japan. Science, 286, 937–939.

Ranero, C.R. and Sallares, V. (2004) Geophysical evidence for hydration of the crust and mantle of the Nazca plate during bending at the north Chile trench. Geology, 32, 549–552.

Reynard, B. and Wunder, B. (2006) High-pressure behavior of synthetic antigorite in the MgO-SiO$_2$-H$_2$O system from Raman spectroscopy. American Mineralogist, 91, 459–462.

Reynard, B., Hilairet, N., Balan, E., and Lazzeri, M. (2007) Elasticity of serpentines and extensive serpentinization in subduction zones. Geophysical Research Letters, 34, L13307, DOI: 10.1029/2007GL030176.

Richet, P. and Gillet, P. (1997) Pressure-induced amorphization of minerals: a review. European Journal of Mineralogy, 9, 907–933.

Salje, E.K.H., Carpenter, M.A., Malcherek, T., and Boffa Ballaran, T. (2000) Autocorrelation analysis of infrared spectra from minerals. European Journal of Mineralogy, 12, 503–519.

Schmidt, M.W. and Poli, S. (1998) Experimentally based water budget for dehydrating slabs and consequences for arc magma generation. Earth and Planetary Science Letters, 163, 361–379.

Scott, H.P., Liu, Z., Hemley, R.J., and Williams, Q. (2007) High-pressure infrared spectra of talc and lawsonite. American Mineralogist, 92, 1814–1820.

Serna, C.J., White, J.L., and Velde, B.D. (1979) The effect of aluminum on the infrared spectra of 7 Å trioctahedral minerals. Mineralogical Magazine, 43, 141–148.

Shinoda, K., Yamakata, M., Nanba, T., Kimura, H., Moriwaki, T., Kondo, Y., Kawamoto, T., Niimi, N., Miyoshi, N., and Aikawa, N. (2002) High-pressure phase transition and behavior of protons in brucite Mg(OH)$_2$: A high-pressure–temperature study using IR synchrotron radiation. Physics and Chemistry of Minerals, 29, 396–402.

Stolper, E. (1982) Water in silicate glasses: An infrared spectroscopic study.

Contributions to Mineralogy and Petrology, 81, 1–17.

Uehara, S. and Shirozu, H. (1985) Variations in chemical composition and structural properties of antigorites. Mineralogical Journal, 12, 299–318.

Ulmer, P. and Trommsdorff, V. (1995) Serpentine stability to mantle depths and subduction-related magmatism. Science, 268, 858–861.

Velde, B. and Martinez, G. (1981) Effect of pressure on OH-stretching frequencies in kaolinite and ordered aluminous serpentine. American Mineralogist, 66, 196–200.

Wunder, B. and Schreyer, W. (1997) Antigorite: high-pressure stability in the system MgO–SiO_2–H_2O (MSH). Lithos, 41, 213–227.

Wunder, B., Wirth, R., and Gottschalk, M. (2001) Antigorite: pressure and temperature dependence of polysomatism and water content. European Journal of Mineralogy, 13, 485–495.